1 **Measurement Report: Rapid changes of chemical characteristics and health risks for high**

2 **time-resolved trace elements in PM$_{2.5}$ in a typical industrial city in response to stringent**

3 **clean air actions**

4 Rui Li[a] [*], Yining Gao[a], Yubao Chen[a], Meng Peng[b c *], Weidong Zhao[c *], Gehui Wang[a], Jiming Hao[b]

5 *[a] Key Laboratory of Geographic Information Science of the Ministry of Education, School of*

6 *Geographic Sciences, East China Normal University, Shanghai, 200241, PR China*

7 *[b] State Key Joint Laboratory of Environment Simulation and Pollution Control, School of*

8 *Environment, Tsinghua University, Beijing, 100084, P.R. China*

9 *[c] Institute of energy conservation and environmental protection, China Electronic Information*

10 *Industry Development Research Institute, Beijing, 100084, P.R. China*

11 *** Correspondence to:**

12 Prof. Li (rli@geo.ecnu.edu.cn), Dr. Peng (mvponesky@163.com), and Prof. Zhao

13 (zhaoweidong@ccidthinktank.com)

14 **Abstract**

15   Atmospheric trace metals entail significant damages in human health and ecosystem safety, and

16 thus a series of clean air actions have been implemented to decrease the ambient element

17 concentrations. Unfortunately, the impact of these emission control measures on element

18 concentrations in fine particles remained poorly understood. In our study, the random forest (RF)

19 model was applied to distinguish the effects of emission and meteorology to trace elements in PM$_{2.5}$

20 in a typical industrial city named Tangshan based on a three-year (2017-2020) hourly field

21 observation. The result suggested that the clean air actions have facilitated the dramatic decreases

22 of the deweathered concentrations of Ga, Co, Pb, Zn, and As by 72%, 67%, 62%, 59%, and 54%,

23 respectively. It is attributable to the strict implementation of "coal to gas" strategies and

24 optimization of industrial structure and layout. However, the deweathered levels of Ca (8.3%), Cr

25 (18.5%), and Fe (23%) only displayed minor decreases, indicating that the emission control

26 measures for ferrous metal smelting and vehicle emission were not very effective. The positive

27 matrix factorization (PMF) results suggested that the contribution ratios of biomass burning, non-

28 ferrous metal smelting, coal combustion, ferrous metal smelting, heavy oil combustion, and traffic-

29 related dust changed from 33%, 11%, 15%, 13%, 3%, and 25% to 33%, 8%, 8%, 13%, 4%, and

30 33%, respectively. To date, no significant noncarcinogenic and carcinogenic risks were observed

31 for all of the elements, while both of As and Pb still showed relatively high health damages. It was

32 proposed to further cut down the combustion-related emissions (e.g., As and Pb) because it showed

33 the highest marginal health benefits. Besides, the control of traffic-related emissions might be a key

34 abatement strategy to facilitate the reduction of elements in fine particles.

35 **Keywords:** hourly trace elements; chemical characteristics; health risks; clean air actions; Tangshan

36 **1. Introduction**

37   Along with the rapid economic development and accelerated urbanization, the energy

38 consumption and output of various industrial products worldwide displayed the persistent increases,

39 thereby leading to the massive emissions of elements especially trace metals into the atmosphere

40 (Tian et al., 2015; Zhu et al., 2020). These elements injected into the atmosphere could pose great

41 threaten to the terrestrial and aquatic ecosystem via dry/wet deposition and then endanger human

42 health through the physiochemical transfer and bioaccumulation in food chains (Fernandez et al.,

43 2000; Harmens et al., 2010; Storelli, 2008). For instance, some toxic trace metals including

44 cadmium (Cd), lead (Pb), and mercury (Hg) were often regarded as human carcinogens even in trace

45 amounts (Micheline et al., 2019; Olujimi et al., 2015). Besides, the excessive accumulation of some

46 biological essential elements such as copper (Cu), iron (Fe), and zinc (Zn) could initiate activation

47 of inflammatory cascades in tissues and the induction of biochemical synthesis pathways by

48 catalyzing the generation of reactive oxygen species (ROS) (Alies et al., 2013; Lopez-Cruz et al.,

49 2016; Saffari et al., 2014), though minor enrichment of these elements was beneficial to the human

50 health and plant growth (Oldani et al., 2017). Apart from the health impacts, some transition metals

51 (e.g., Ni, Zn) could catalyze some chemical reactions such as particle-phase sulfate generation and

52 heterogeneous production and removal of gas-phase hydrogen oxide radicals (HO_x) to aggravate the

53 haze formation (Clements et al., 2013; Guo et al., 2014). Therefore, it is highly imperative to

54 recognize the pollution status of elements in the atmosphere, to identify the major sources and then

55 to propose effective controls measures to alleviate their negative effects on air pollution and human

56 health especially in some developing countries.

In the past decades, hundreds of studies investigated the pollution levels of elements and revealed their sources in various study regions including urban (Das et al., 2018; Duan and Tan, 2013; Lyu et al., 2017; Grivas et al., 2018; Clements et al., 2014), marine (Shi et al., 2015; Witt et al., 2006), mountain (Kang et al., 2016). Most of these studies used the filter sampling (one sample or two samples each day) technique coupled with offline analysis using inductively coupled plasma mass spectrometry (ICP-MS) or inductively coupled plasma-atomic emission spectrometry (ICP-AES) to determine the element concentrations in the atmosphere (Ao et al., 2019; Lin et al., 2016). Although these studies have obtained many valuable information about the occurrence levels and key sources of ambient elements, the low time-resolution data cannot accurately reflect the dynamic transformation and evolution of ambient elements. It was well known that atmospheric emissions, transport and deposition significantly relied on rapidly evolving meteorological conditions (Holden et al., 2016; Rasmussen, 1998), and thus the offline samples inevitably ignored the impacts of environmental shifts with rapid temporality on the atmospheric element concentrations. Moreover, most of current source apportionment studies employed the receptor models (positive matrix factorization (PMF)) to determine the potential sources of elements (Jeong et al., 2016; Lyu et al., 2017), and the accuracy of these models was strongly dependent on the sample size and time resolution (Liu et al., 2018b). In this regard, the high time-resolved observation of atmospheric elements provided an unprecedented opportunity to characterize the occurrence levels, identify their major sources, and assess the health impacts.

To date, only a few studies applied the high-resolution devices to capture the hourly variability of ambient elements. Prati et al. (2000) firstly used Particle Induced X-ray Emission (PIXE) measurements to analyze hourly trace elements in Genoa in Italy. Following this work, A. D'Alessandro et al. (2003) and Dall'Osto et al. (2013) also employed the same technique to determine the trace metals in Italian towns and Barcelona, respectively. Later on, Jeong et al. (2016) used Xact metals monitor to reveal the temporal variability of atmospheric elements in Toronto, Canada in summer and winter during 2013-2014. Recently, the Xact metals monitor has begun to be performed in China due to the higher accuracy and convenience. Chang et al. (2018) firstly used the online multi-element analyzer to achieve a one-year near real-time observation of ambient elements in China and found traffic, nonferrous metal smelting and coal combustion were major

86 sources of atmospheric trace metals. Afterwards, Cui et al. (2019) applied the analyzer to monitor

87 1-year atmospheric elements, and demonstrated that dust, industry, and biomass burning were

88 considered as the dominant sources of most trace elements in Beijing, accounting for 36%, 10.7%,

89 and 27% of total $PM_{2.5}$ concentration, respectively. Up to date, continuous hourly element

90 observation was only performed less than one year in most of the previous studies, and the long-

91 term temporal variability of absolute concentrations and key pollution sources of atmospheric

92 elements cannot be fully revealed.

93 Since 2013, Chinese government proposed strict Air Pollution Prevention and Control Action

94 Plan (the Action Plan) across China and the emissions of multiple gaseous pollutants suffered from

95 significant decreases. In turn, the absolute concentrations and health effects of air pollutants also

96 experienced the rapid changes response to these stringent control measures. Zhang et al. (2019)

97 reported that the population-weighted annual mean $PM_{2.5}$ concentration decreased from 62 to 42

98 $\mu g/m^3$ during 2013-2017 and reduced $PM_{2.5}$-attributable premature deaths by 0.4 million due to the

99 impact of the Action Plan. Shortly after that, Geng et al. (2019) estimated that the population-

100 weighted mean concentrations of SO_4^{2-}, NO_3^-, and NH_4^+ in $PM_{2.5}$ decreased from 11.1, 13.8, and

101 7.4 $\mu g/m^3$ to 6.7, 13.1, and 5.8 $\mu g/m^3$, respectively during the same period. Nevertheless, the impact

102 of the Action Plan on trace elements in fine particles still remained poorly understood. Especially,

103 the knowledge about the variation of source apportionment and health risks for trace elements

104 response to the Action Plan was extremely limited. Moreover, most of the previous studies only

105 utilized the original concentrations to analyze the impact of clean air policy (He et al., 2021; Xiao

106 et al., 2020). It was well known that the pollutant concentrations in the atmosphere were affected

107 by meteorology and anthropogenic emissions simultaneously (Li et al., 2021), and the use of original

108 element concentrations alone cannot assess the unique contribution of emission reduction to the air

109 pollutants. Thus, it is urgently needed to remove the effect of meteorology and accurately capture

110 the independent influence of the Action Plan on the chemical characteristics, source apportionment,

111 and health risks of trace elements. Such knowledge is critical to design effective air pollution

112 mitigation strategies in the near future.

113 As a heavily industrialized city located in North China Plain (NCP), Tangshan possesses many

114 energy-intensive industries including coal-fired power plants, non-ferrous smelting industries,

115 textiles, building materials, chemical engineering, and papermaking industries (Ren et al., 2011).

116 Intensifying industrial development and urbanization aggravated local air quality. Previous studies

117 performed in Tangshan focused on the trace metals in soils and dusts (Cui et al., 2020; Song et al.,

118 2011), whereas no study analyzed the long-term and high-resolution variabilities of atmospheric

119 elements. Since 2013, many emission control measures such as the establishment of desulfurization

120 and denitration facilities for coal-fired power sector have been strictly implemented in Tangshan

121 (Ma et al., 2019). Especially after 2017, coal to gas project has started to be implemented in

122 Tangshan and the energy structure suffered from significant change (Wang et al., 2020b). In

123 response to substantial pollution control policies, the chemical compositions and major sources of

124 trace elements might show corresponding change. Here, we conducted a near real-time

125 measurement of atmospheric elements in $PM_{2.5}$ using a Xact multi-metals analyzer in Tangshan,

126 China during September 2017 to August 2020. The primary objectives of our study were to (1)

127 determine the occurrence levels of elements in $PM_{2.5}$ of Tangshan; (2) to analyze the seasonal and

128 intra-week variations of atmospheric elements and to distinguish the separate contributions of

129 emission and meteorology to these species; (3) to quantify the changes of major sources for

130 atmospheric elements during this period; (4) to assess the changes of health risks in response to

131 these pollution control measures.

132 **2. Material and methods**

133 2.1 Sampling site

134 　　The sampling site (39.66°N, 118.18°E) is situated on the rooftop (~20 m above the ground) of a

135 building in the urban district of Tangshan and no high buildings spread around within 100 m range.

136 The sampling site is close to some major roads including Airport Road, Huayan North Road, and

137 Changhong Road. A large number of commercial streets and recreation facility surround the site.

138 Although no big industrial point source was closely adjacent to the sampling site, many potential

139 pollution sources were located more than 15 km away from the site. For instance, Beihu industrial

140 region is located about 15 km in the eastern direction of the site. Some large iron steel industries

141 and nonferrous/ferrous smelting industries were located on the north of sampling site (more than 30

142 km). Besides, most of large petrochemical industries, coal-fired power plants, and shipping

143 industries focus on Caofeidian and Haigang developing zones, both of which were located about 50

144   km in the South area of the sampling site. The detailed location is depicted in Figure 1.

145   2.2 Instrumentation

146   Hourly mass concentrations of 22 elements, including Ag, As, Au, Ca, Co, Cu, Cd, Cr, Fe, Ga,

147   Hg, K, Mn, Ni, Pb, Pd, Sb, Se, Sn, Tl, V, and Zn in $PM_{2.5}$ were determined by an online multi-

148   element analyzer (Model Xact 625, Cooper Environment Service, USA) (Table S1). The sample air

149   is drawn through a small spot on the tape where the $PM_{2.5}$ was collected at a flow rate of 16.7 L

150   min^{-1} during September 2017-August 2020. An internal Pd pod is utilized as an internal standard to

151   detect the stability of the instrument. Tl was removed from the datasets because over 95% of their

152   concentrations were below the limit of detection (LOD) (Table S2). Au, Cd, Sn and Sb were also

153   excluded from the datasets because over 50% of the concentrations for these metals were below the

154   LOD. To validate the reliability of online multi-element analyzer, many previous studies used the

155   filter sampling coupled with ICP-MS and ICP-AES to determine the daily concentrations of

156   elements and confirmed that the online device showed good agreement with the filter sampling

157   (Furger et al., 2017; Tianxue et al., 2006). Hourly averaged meteorological parameters including air

158   temperature (T), relative humidity (RH), air pressure (P), wind direction (WD), and wind speed

159   (WS) during the sampling period were measured by a weather station with sonic anemometer

160   (150WX, Airmar, Milford, NH, USA). The hourly mass concentration of $PM_{2.5}$ was determined by

161   the particulate monitor (Thermo, FH62C-14). The routine procedures, including the daily zero or

162   standard calibration, span and range check, station environmental control and staff certification,

163   followed the Technical Guideline of Automatic Stations of Ambient Air Quality in Tangshan based

164   on the national specification HJ/T193-2005, which was revised based on the technical guidance

165   established by the US EPA. Quality Assurance and Quality Control (QA/QC) for the Xact

166   measurements was implemented throughout the sampling period. The internal Pd upscale value was

167   recorded after daily programmed test for the instrument.

168   2.3 Deweathered model development

169   The concentrations of air pollutants were affected by meteorological parameters and emissions

170   simultaneously. In order to separate the contributions of emissions, the impacts of meteorological

171   conditions must be eliminated. In this study, a typical machine-learning model named random forest

172   (RF) approach was applied to distinguish the effects of emissions and meteorological conditions

设置了格式: 下标

6

173   (Chen et al., 2018). All of trace elements in $PM_{2.5}$ were treated as the dependent variables. The time

174   predictors (year, day of year (DOY), day of week (DOW), hour of day (HOY)) and meteorological

175   factors including air temperature (T), relative humidity (RH), wind speed (WS), wind direction

176   (WD), and air pressure (P) were regarded as the predictors (Figure S1). The original dataset was

177   randomly classified into a training dataset (80% of input dataset) for developing the RF model and

178   the remained one was treated as the test dataset. After the building of the RF model, the deweathered

179   technique was employed to predict the concentrations of trace elements at a specific time point. The

180   deweathered element concentrations served as the concentrations contributed by emission alone.

181   The differences of original element concentrations and deweathered element concentrations were

182   regarded as the concentrations contributed by meteorology. Many statistical indicators including R^2

183   value, root-mean-square error (RMSE), and mean absolute error (MAE) were regarded as the major

184   indicators to evaluate the RF modelling accuracy. The RF model with the 5-fold cross-validation R^2

185   value less than 0.5 was considered to be the unconvincing result and cannot reflect the impacts of

186   emission and meteorology on air pollutants accurately because more than 50% variability of the

187   training model cannot be appropriately explained. After the model evaluation, only the trace

188   elements with the cross-validation R^2 values larger than 0.5 were selected to estimate the respective

189   contributions of emission and meteorology to the total element concentrations.

190   2.4 PMF model

191   As a typical receptor model applied to source apportionment, PMF 5.0 version was used to

192   identify the major origins of atmospheric elements and to determine the contribution ratio of each

193   source to these elements. The objective of PMF is to solve the issues of chemical mass balance

194   between measured concentration of each element and its source contributions by decomposing the

195   input matrix into factor contribution and factor profile. The detailed equation is shown in Eq. (1).

196   Besides, the contribution of each source for individual element must be non-negative because no

197   sample has a negative source contribution. In brief, the basic principle of PMF is to calculate the

198   least object function Q when the g_{ik} must be a positive-definite matrix based on Eq. (2) (Paatero and

199   Tapper, 1994; Reff et al., 2007).

200
$$x_{ij} = \sum_{k=1}^{p} g_{ik} f_{kj} + e_{ij} \quad (1)$$

$$Q = \sum_{i=1}^{n} \sum_{j=1}^{m} [\frac{x_{ij} - \sum_{k=1}^{p} g_{ik} f_{kj}}{u_{ij}}]^2 \quad (2)$$

where x_{ij} and e_{ij} denote the concentration and uncertainty of jth element, respectively. g_{ik} represents the contribution ratio of kth source to ith sample, f_{kj} represents the ratio of jth element in kth source, and e_{ij} indicates the residual of jth element in the i sample. The uncertainties associated with factor profiles were evaluated using three error calculation methods including bootstraps (BS) method, displacement (DISP) analysis, and the combination method of DISP and BS (BS-DISP). For the BS method, 100 runs were performed and the result has been believed to be valid since all of the factors showed a mapping of above 90%. DISP analysis also confirmed that the solution was considered to be stable because the observed drop in the Q value was less than 0.1% and no factor swap occurred. For the BS-DISP analysis, the solution has been verified to be useful because the observed drop in the Q value was less than 0.5%. Furthermore, both of the results from BS and BS-DISP did not suggest any asymmetry or rotational ambiguity for all of the factors (Manousakas et al., 2017; Taghvaee et al., 2018).

2.5 Health risk assessment of trace metals in $PM_{2.5}$

As a typical industrial city, Tangshan possesses a large number of residents and poor air quality. Therefore, the residents in Tangshan might suffer from severe exposure risks of trace metals. In our work, the carcinogenic and non-carcinogenic risks of trace metals in $PM_{2.5}$ were evaluated based on some statistical threshold proposed by International Agency for Research on Cancer (IARC). Based on the criterion of IARC, As, Ni, Cr, and Pb were considered to be carcinogenic to humans.

The carcinogenic and non-carcinogenic risks induced by meatal exposure for adults and children were evaluated based on the carcinogenic risks (CR) and hazard quotient (HQ). The formulas for calculating ADD, CR, and HQ are as follows:

$$ADD=(C \times InhR \times EF \times ED)/(BW \times AT) \quad (3)$$

$$HQ=ADD/RfD \quad (4)$$

$$CR = ADD \times CSF \quad (5)$$

where C (mg m^{-3}) denotes the concentration of the corresponding trace metal in $PM_{2.5}$; InhR is the respiratory rate; EF represents the annual exposure frequency (d y^{-1}); ED is the exposure duration; BW is the average body weight; AT denotes the average exposure time; ADD means the daily intake

8

229 (mg/kg/day) of trace metals; RfD represents the reference dose, calculated with reference

230 concentrations; CSF is the cancer slope factor. The potential non-carcinogenic risk of the trace metal

231 ~~is considered to be~~might be high when HQ was above 1.0, whereas the health risk is not obvious

232 when HQ is below 1.0. The carcinogenic risk of each trace metal is evaluated based on whether CR

233 is higher than 10^{-4}.

3. Results and discussion

3.1 Occurrence levels and inter-annual variations of original element concentrations

236   The total mass concentrations of 16 elements in $PM_{2.5}$ of Tangshan varied between 230 ng/m^3

237 to 20000 ng/m^3, with the median value of 3100 ± 900 ng/m^3. The total element concentrations in

238 Tangshan accounted for 5.7% of the total mass concentrations of $PM_{2.5}$, which was slightly higher

239 than those in Beijing (4.7%) and Qingdao (4.0%), and significantly higher than that in Shanghai

240 (1.80%) (Chang et al., 2018; Cui et al., 2019). As depicted in Figure 2, the concentrations of these

241 elements followed the order of K (1400 ± 950 ng/m^3) > Fe (880 ± 590 ng/m^3) > Ca (330 ± 270

242 ng/m^3) > Zn (320 ± 160 ng/m^3) > Pb (58 ± 36 ng/m^3) > Mn (54 ± 32 ng/m^3) > Cu (22 ± 19 ng/m^3) >

243 As (15.3 ± 11.0 ng/m^3) > Se (6.5 ± 5.3 ng/m^3) > V (4.0 ± 3.6 ng/m^3) > Cr (2.8 ± 2.2 ng/m^3) > Ag

244 (2.8 ± 2.1 ng/m^3) > Ni (2.2 ± 1.8 ng/m^3) > Hg (1.5 ± 0.8 ng/m^3) > Ga (0.9 ± 0.7 ng/m^3) > Co ($0.7 \pm$

245 0.2 ng/m^3). Among all of these elements, K, Fe, Zn, and Ca were most abundant species, accounting

246 for 95% of the total elements in $PM_{2.5}$. The remaining element concentrations only accounted for

247 less than 6% of the total element concentrations, which was similar to the previous studies (Chang

248 et al., 2018; Cui et al., 2019). Nearly all of the trace elements in Tangshan, Beijing, Qingdao, and

249 Shanghai were significantly lower than those in Zibo during 2006-2007 (Table S3). It suggested

250 that the trace elements in China experienced marked decreases in the past decades (Zhang et al.,

251 2018). Compared with some cities in some developed countries, all of the trace element

252 concentrations were significantly higher than those in London and Toronto. However, the

253 concentrations of K, Ca, V, Cr, Mn, and Fe in Tangshan were higher than those in Venice, Italy.

254   Due to the higher exposure risk and great threaten to human health, it is necessary to compare

255 the trace metal concentrations with the risk threshold proposed by many organizations or countries.

256 As shown in Table 1, we have collected many risk thresholds in different countries and found that

257 the Hg (1.5 ± 0.8 ng/m^3), Ni (2.2 ± 1.8 ng/m^3), and Pb concentrations (58 ± 36 ng/m^3) in Tangshan

were significantly lower than the thresholds of the Chinese Ambient Air Quality Standard (CAAQS) (Hg: 50 ng/m^3), World Health Organization (WHO) (Hg: 1000 ng/m^3, Ni: 25 ng/m^3, and Pb: 1000 ng/m^3), Europe Union (EU) (Ni: 20 ng/m^3), and the United States (Pb: 150 ng/m^3). However, both of the As (15 ± 11 ng/m^3) and Cr concentrations (2.8 ± 2.2 ng/m^3) in PM$_{2.5}$ of Tangshan were much higher than the standard values of CAAQS (As: 6.0 ng/m^3 and Cr: 0.03 ng/m^3), WHO (As: 6.6 ng/m^3 and Cr: 0.25 ng/m^3), and EU (As: 6.0 ng/m^3).

The inter-annual variation of original concentrations of trace elements in PM$_{2.5}$ are depicted in Figure 3 and S2-S3. The original concentrations of all the trace elements exhibited the decreasing trends. Cu, Co, Zn, Pb, As, and Ga concentrations suffered from dramatic decreases from 37 to 12 ng/m^3 (68%), 1.21 to 0.4 ng/m^3 (66%), 400 to 190 ng/m^3 (53%), 71 to 40 ng/m^3 (44%), 20 to 11 ng/m^3 (44%), and 1.09 to 0.6 ng/m^3 (42%), respectively. Following these species, observed K (40%), Ag (39%), V (39%), Ni (36%), Ca (33%), Mn (29%), Se (29%), Fe (27%), and Cr (21%) concentrations showed moderate decreasing ratios. The observed Hg level exhibited the lowest decreasing ratio from 1.59 to 1.43 ng/m^3 (9.9%).

3.2 Impact of emission reduction on trace element concentrations

Although the original concentrations of trace elements could be utilized to analyze the impact of the clean air policy, the role of emission reduction on element concentration might not be clearly clarified because the meteorological factors were also important variables affecting the air quality. In order to accurately reflect the response of element concentrations to emission reduction alone during 2017-2020, the meteorological conditions were eliminated by RF model in our study. Based on the results in Figure S4, the RF models for all of the species showed better performance because their R^2 values were higher than 0.50, and the slopes of all of the fitting curves were also close to the R^2 values. The result suggested that the separation of meteorology and emission of trace elements based on RF model was reliable. During 2017-2020, the deweathered concentrations of Ga, Co, Pb, Zn, and As showed the rapid decreases from 1.52 to 0.4 ng/m^3 (72%), 1.31 to 0.4 ng/m^3 (67%), 92 to 35 ng/m^3 (62%), 410 to 170 ng/m^3 (59%), and 21 to 10 ng/m^3 (54%), respectively (Figure 3). It was well known that As, Co, and Pb were typical marker elements for coal combustion and the "coal-to-gas" and "coal-to-electricity" strategies have been widely performed in Tangshan (Fang et al., 2020; Li et al., 2017). Wang et al. (2020a) has estimated that these effective control

287　measures have contributed to around 60% of the total PM$_{2.5}$ reductions. Meanwhile, the upgradation

288　and optimization of industrial structure/layout and the shutdown of high-pollution industries were

289　also strictly implemented in Tangshan, and thus led to the dramatic decreases of Ga and Zn

290　concentrations because Ga and Zn were common forms of nonferrous metal smelting (Tian et al.,

291　2015). However, the deweathered Ca level displayed the lowest decrease ratio (8.3%) from 2017 to

292　2020, indicating that clean air actions cannot significantly reduce the fugitive emissions. In addition,

293　the deweathered Fe (23%) and Cr (18.5%) also suffered from relatively low decrease ratios. It was

294　well documented that Fe and Cr originated from metallurgical industry such as steel production and

295　ferrous metal smelting (Tian et al., 2015), and the slight decreases of deweathered Fe and Cr levels

296　during the sampling period suggested that the emission control measures for ferrous metal smelting

297　should be strengthened in the future work.

298　　In addition, the decreasing ratios of the deweathered concentrations for each species displayed

299　different seasonal characteristics. The deweathered concentrations of some elements related with

300　industrial activities (e.g., Ga, Zn, and Cr) suffered from rapid decreases in autumn and winter

301　compared with other seasons during 2017-2020 (Figure 4), indicating that the optimization of

302　industrial layout and shutdown of outdated industries were effective to decrease these element

303　emissions especially in high-pollution season. Some elements derived from biomass burning

304　including K (66%) and Se (50%) also suffered from the most dramatic decreasing ratios in autumn.

305　It was assumed that enhanced crop residual burning occurred frequently during the autumn harvest

306　season. Ke et al. (2019) confirmed that the number of fire spots in October-November was even

307　higher than that in June and the burned area in harvest season was highest during 2013-2017.

308　However, the control on open biomass burning has been implemented strictly in recent years, largely

309　reducing the K and Se emissions in autumn. It should be noted that the deweathered Pb (46%), Co

310　(65%), and As (45%) concentrations in winter did not display high decreasing ratios though the

311　annual mean deweathered Pb, Co and As levels experienced dramatic decreases. The result revealed

312　that it was still difficult to reduce the Pb, Co, and As emissions during the heating season because

313　increased coal consumption for domestic heating largely offset the contributions of emission control

314　measures (Zhu et al., 2018; Zhu et al., 2020).

315　　Apart from the seasonal difference of each species, the decreasing ratios of these elements also

11

suffered from distinctly intra-weekly variations. The deweathered concentrations of most elements except Ca, Cu, Ni, and V exhibited the higher decreasing ratios at the weekends than those in the weekdays (Figure 5). Cui et al. (2020) has demonstrated that the weaker supervision on industrial enterprises on weekends could lead to the higher concentrations of non-traffic elements such as K, As, Se, and Cr in some cities. Fortunately, grid monitoring has been widely performed in Tangshan recently (http://hbepb.hebei.gov.cn/hbhjt/xwzx/jicengfengcai/101624062321621.html), and many low-cost sensors were installed at some energy-intensive industries, which could decrease the stealing emissions of some elements. Nonetheless, the decreasing ratios of Ca, Cu, V, and Ni did not show the regular intra-weekly characteristics. In recent years, Tangshan adopted strict traffic management regulation and the nonlocal light duty vehicles were restricted to drive inside the urban area one day per week based on the end number of the license plates (Westerdahl et al., 2009; Wu et al., 2011), whereas the restrictions were not valid at weekends (Liu et al., 2007). Theoretically, the traffic control should result in marked decreases of traffic-related element concentrations on weekdays compared with weekends. However, in our study, some traffic-related elements such as Ca and Cu did not show similar characteristics. Meanwhile, as the important tracer of vehicle emission, the NO_x concentration in Tangshan did not show regular intra-weekly pattern. It was supposed that the vehicle volume in Tangshan has increase from 2.0 to 2.4 million (http://tjj.hebei.gov.cn/), which largely offset the benefits of traffic controls. The shipping-related elements including Vi and Ni also did not show regular intra-weekly variation because no similar heavy metal emission control measures for shipping were performed.

3.3 The role of meteorology on the year-to-year variations of element concentrations

The difference of original and deweathered element concentrations could be regarded as the concentrations contributed by meteorological parameters. The positive impacts of meteorological parameters on trace elements suggested that the meteorological conditions were unfavorable to the pollutant diffusion, while the negative impacts of meteorological indicators meant the favorable condition to trace elements. In our study, the roles of meteorological conditions on Ca (-25%), V (-10%), Cr (-2.5%), Mn (-0.7%), Fe (-4.6%), Ni (-7.6%), and Cu (-21%) during 2017-2020 were negative (Figure S5), while the roles of meteorological parameters on other elements were positive. The result suggested that those elements derived from vehicle emission (Ca, Cu, and Fe), ferrous

12

metal smelting (Cr and Mn), and heavy oil combustion (V and Ni) were less sensitive to the emission reduction actions compared with other elements and the meteorological conditions were much beneficial to the diffusion of these elements. In order to further reveal the key meteorological factors for these elements, we used RF model to calculate the variable importance of all of these meteorological parameters including P, RH, T, WD, and WS. The result suggested that Ca, Fe, and Cu were mainly influenced by T, whereas V, Ni, Cr, and Mn were often associated with WD and WS (Figure 6). During the spring and summer in 2017-2020, the average air temperature decreased from 8.9 and 27 to 7.2 and 26°C, respectively. The decreased air temperature led to the higher water content in the soil and a lower tendency of dust suspension, and might decrease the concentrations of Ca, Fe, and Cu (Manju et al., 2018; Yang et al., 2017; Lyu et al., 2016). Although the annual average wind speed in Tangshan decreased from 1.70 to 1.45 m/s, the mean wind speed from the southeastern direction displayed slight increase from 1.34 to 1.50 m/s. Zhao et al. (2013) verified that V and Ni were usually emitted from heavy oil combustion of ocean-going ship engines. Many coastal ports and ferrous metal smelting industries were located on the southeastern direction of the sampling site, and thus the enhanced WS might promote the dilution and dispersion of trace elements (Figure S6-8). As shown in Figure S8, both of V and Ni showed the higher concentrations in the southeastern part of Tangshan and the concentrations displayed gradual decreases along the Southeast-Northwest transect, which also demonstrated that both of V and Ni in the sampling site could be derived from coastal shipping emission.

3.4 The impact of clean air policy on source apportionment of trace elements

Although the major sources of elements could be determined based on some important tracers (e.g., K, V), the contributions of major sources to each element still remained unknown. Therefore, Positive matrix factorization (PMF 5.0) version was applied to identify more source information of elements in PM$_{2.5}$ during 2017-2020 based on deweathered levels. After 20 runs, more than 26000 samples were trained to determine the optimal six factors with the lowest values of Q (robust) and Q (true). The BS, DISP, and BS-DISP methods confirmed that the most reliable solution was obtained with six factors. The detailed information of PMF analysis and error diagnostics are summarized in Table S4-6.

As shown in Figure S9, the trace elements in PM$_{2.5}$ during 2017-2018, 2018-2019, and 2019-

13

374 2020 showed similar cluster characteristics. Factor 1 possesses high loadings of K (55%) and Se

375 (42%). K and Se were often regarded as the major tracers of biomass burning. Due to the increasing

376 usage of biomass fuels for domestic heating during the heating season, K, and Se in $PM_{2.5}$ of

377 Tangshan showed the higher values in winter, suggesting that these metals in fine particles could

378 originate from the combustion of biomass fuels. Except the domestic heating, we found some

379 episodes during harvesting season in late summer (2450 and 11.2 ng/m^3) and early autumn (2630

380 and 9.5 ng/m^3) also showed extremely high concentrations of K, which might be linked with local

381 open biomass burning (Chen et al., 2017). Based on the map of fire points and backward air masses

382 trajectories (Figure S7S6-8), the metals released from biomass burning or open waste incineration

383 in NCP could be transported to the sampling site by the dominant southerly wind, which further

384 proved the impacts of open biomass burning (Chen et al., 2017).

385 The abundant elements in factor 2 included Ag (53%), Zn (51%), and Cu (36%). Owing to the

386 higher temperatures during the roasting, sintering and smelting processes for the extraction of Cu,

387 and Zn from ores, some metals such Ag in nonferrous metal ores could be vaporized as the

388 byproduct and released into the flue gas (Pacyna and Pacyna, 2001; Wu et al., 2012). Therefore, the

389 factor 2 was interpreted as the non-ferrous metal smelting source.

390 Factor 3 was characterized by a large mass fraction of Co (81%), Pb (61%), Hg (57%), and As

391 (39%). After the phase-out of leaded gasoline since 1980s, the contribution from coal combustion

392 to Pb suffered from rapid increase and accounted for the major fraction of particulate Pb (Das et al.,

393 2018). Meanwhile, Co and Hg were also treated as the important byproducts released from coal

394 burning and the Co and Hg concentrations often increased significantly with the elevation of burning

395 temperature (Tang et al., 2018). Tian et al. (2015) estimated that 73% of As, 56 % of Pb, and 47 %

396 of Hg were found to be emitted from coal combustion in China. Coal consumption in South China

397 was mainly driven by coal-fired power plants, while the coal-based heating was the major sector for

398 the coal consumption in NCP. In our study, As, Co and Pb showed the higher concentrations in

399 winter (heating season) (18.7, 0.9, and 76 ng/m^3) compared with other seasons (14, 0.6, and 51

400 ng/m^3). The markedly seasonal discrepancies of As, Co and Pb strongly supported the impact of the

401 coal combustion for domestic heating on the enhancement of As, Co and Pb in the fine particles.

402 Factor 4 was distinguished by high loadings of Cr (78%) and Mn (39%), respectively. Cr and

Mn were mainly sourced from metallurgical industry such as steel production and ferrous metal smelting (Liu et al., 2018a; Tian et al., 2015; Zhu et al., 2018). China occupied more than 49% of world steel production in 2017 (approximate 830 million tons), and 60% large steel producers were located in China (Chang et al., 2018). Tangshan possesses many large steel production industries such as Tangshan Steel, Qian'an Steel, and Guofeng Steel. Besides, some industries of Capital Steel have been migrated into Tangshan (Li et al., 2019), which might increase the Cr and Mn emissions.

Factor 5 explained 10.1% of the total species and it was characterized by high loadings of V (88%) and Ni (51%). It was well documented that V was a key fingerprint of heavy oil combustion, which was generally emitted from shipping emission and petrochemical refining (Shafer et al., 2012). However, Ni was widely utilized as a tracer of fuel oil combustion in industries (Zhu et al., 2018). Many oil-fired power plants were located in Tangshan for central heating (Yu et al., 2013). Based on the backward trajectory and wind direction (Figure S7S6-S10S8), we found that high concentrations of V and Ni might be derived from the southeastern air masses especially in summer and autumn, indicating the impacts of coastal port and petroleum refinery industry. In addition, both of V and Ni concentrations displayed the gradual decreases along the Southeast-Northwest transect, indicating the potential sources were located on Southeast Tangshan (Figure S8). Gathering evidence suggested that the V/Ni ratio in petroleum coke with a low-sulfur content and fuel oil usage ranged from 1 to 3 (Moreno et al., 2010). The annual mean ratios of V and Ni in our study reached 1.2 during the sampling period, which was in the range of this interval. The result also revealed that petrochemical refining and heavy oil combustion derived from coastal shipping emission might be an important source of V and Ni the fine particles.

Factor 6 was characterized by high loadings of Ca (78%), Cu (32%), and Fe (33%), and moderate loadings of Mn (31%) and Zn (29%). Some previous studies have demonstrated that both of Cu, Fe, and Zn were released from tyre and brake wear because they were the necessary materials for brake pads and the agents in brake linings (Dall'Osto et al., 2013; Hjortenkrans et al., 2007). Ca was probably sourced from the road fugitive dust because it was one of the most abundant elements in the upper continents (Alves et al., 2015; Liu et al., 2018a). Moreover, we have found Fe, Ca, and Zn displayed remarkably high values during the morning rush hours and a small peak during the sunset (Figure S10), which was coincident to the diurnal variation of traffic volume. Thus, the factor

15

432 6 was identified as the traffic-related dust source.

433 Although six similar sources were revealed during 2017-2020, the contribution concentrations

434 and ratios of these sources varied greatly in these years. As shown in Figure 7 and 8, the contribution

435 concentrations of biomass burning, non-ferrous metal smelting, coal combustion, and ferrous metal

436 smelting to trace elements decreased from 1458, 479, 636, and 569 ng/m^3 to 901, 225, 230, and 345

437 ng/m^3, respectively. However, the contribution concentrations of heavy oil combustion and traffic-

438 related dust displayed slight increase during 2017-2019, while they decreased rapidly after 2019.

439 The contribution concentrations for nearly all of the sources to trace elements suffered from

440 decreases during 2017-2020 because the total deweathered levels of trace elements experienced

441 decreases in the past three years. However, the contribution ratios of these sources to trace elements

442 did not show similar characteristics. For instance, the contribution ratio of traffic-related dust

443 increased from 25% to 33%. However, the contributions of non-ferrous metal smelting and coal

444 combustion decreased from 11% to 8% and 15% to 8%, respectively. The contributions of ferrous

445 metal smelting, heavy oil combustion, and biomass burning remained relatively stable during this

446 period.

447 Due to the strict implementation of clean air policy, many outdated industrial capacities were shut

448 down and the cleaner technologies have been upgraded, which facilitated the production decreases

449 of pig iron and coal-fired power plants (Ma et al., 2019). Hence, the contribution concentrations and

450 ratios of non-ferrous metal smelting and coal combustion experienced dramatic decreases. Although

451 the open biomass burning has been strictly restricted in Tangshan (Chang et al., 2018), the

452 contribution ratios of biomass burning to trace elements in PM$_{2.5}$ remained relatively stable, which

453 might be attributable to the rapid decreases of the contributions derived from coal combustion and

454 non-ferrous metal smelting. In addition, the biofuel combustion was still widespread in some rural

455 and suburb areas (Kamal et al., 2015; Li et al., 2020), which might offset the decreases in the

456 contributions of open biomass burning. Although the contribution concentrations of traffic-related

457 dust to trace elements also showed slight decrease, the contribution ratios of traffic-related dust to

458 some trace elements exhibited the marked increases (8%) during 2017-2020 because the

459 contribution ratios of metal smelting and coal combustion suffered from substantial decreases. The

460 result also demonstrated that the implementation of coal to gas project facilitated the decreases of

461 trace element concentrations. In addition, the source variation trend also suggested that the

462 formulation of many new quality standards for non-road diesel fuels cannot fully decrease the

463 element emissions (Cui et al., 2017), and thus the control of traffic-related dust should be enhanced

464 in the future.

465 3.4 5 Health risk assessment of trace metals in $PM_{2.5}$

466 Although the trace metals only accounted for minor fraction of total mass concentration of $PM_{2.5}$,

467 it might pose a great threaten to the human health because most of these metals were bioavailable

468 and non-degradable (Rai et al., 2019; Yi et al., 2011). Unfortunately, previous studies mainly used

469 the filter sampling techniques to determine the concentrations of trace metals and then assess their

470 health risks (Cui et al., 2018; Huang et al., 2016). These low-resolution data might not accurately

471 reflect the real health risks triggered by metal exposure. In our study, we employed the online data

472 to assess the health risks derived from metal exposure.

473 The health risks of trace metals could be classified into two types including carcinogenic and

474 non-carcinogenic risk. Based on the major parameters summarized in Table S7 and Table S8, we

475 estimated both of the carcinogenic and non-carcinogenic risks of major metals. To evaluate the

476 impacts of emission control measures on element concentrations, both of the health risks based on

477 original element levels and deweathered element concentrations were calculated. The mean CR

478 values based on original concentrations were in the order of Pb (2.3×10^{-6} (adult) and 1.4×10^{-6}

479 (child)) > As (1.9×10^{-6} and 1.1×10^{-6}) > Cr (0.11×10^{-6} and 0.07×10^{-6}). The total CR values for adults

480 and children reached 4.3×10^{-6} and 2.6×10^{-6} (Table 2), respectively. The total CR values were located

481 in the range of the acceptable (10^{-6}) and least stringent risk levels (10^{-4}), which suggested that

482 Tangshan suffered from slight metal carcinogenic risk. Among all of these metals, Pb and As

483 displayed the higher CR values. It was assumed that the coal combustion for domestic heating might

484 be the dominant factor for the higher risks of Pb and As in Tangshan because both of Pb and As in

485 $PM_{2.5}$ were mainly derived from coal combustion. With regard to the non-carcinogenic risks of trace

486 metals, the HQ of As (1.2×10^{-2} and 2.9×10^{-2}) and Pb (6.8×10^{-4} and 17×10^{-4}) showed the higher

487 values compared with other elements. The result indicated that nearly all of the elements did not

488 display potential remarkable non-carcinogenic risk because HQ values of all the metals were less

489 than 1. The total HQ value of these metals were also lower than 1, indicating that the trace elements

17

490 in Tangshan did not show significant non-carcinogenic risk.

491 By removing the impact of meteorological conditions, we can isolate the impact of clean air

492 policy on health risks associated with metal exposure alone. The decrease ratios of CR values based

493 on the deweathered As and Pb concentrations during 2017-2020 were 54% and 62%, respectively

494 (Table 3). However, the decrease ratios of CR values based on original As and Pb levels only

495 reached 44%. The result suggested that the clean air policy in recent years significantly decreased

496 the As and Pb emissions. Additionally, the decrease ratios of HQ values for original Cu (41%) and

497 Zn (53%) were much less than those for deweathered ones (Cu: 47% and Zn: 59%). Nevertheless,

498 some other elements did not show the similar characteristics. For instance, the decrease ratios of

499 HQ values for original Cr (21%) and Fe (27%) were even slightly higher than those for deweathered

500 ones (Cr: 19% and Fe: 23%). It was assumed that the clean air policy in recent years facilitated the

501 emission reduction of non-ferrous metal smelting and coal combustion efficiently. However, the

502 concentrations of elements derived from ferrous metal smelting and vehicle emission did not show

503 marked decreases, which was in good agreement with the source apportionment result in the section

504 3.3. Thus, in the future work, it is highly imperative to further reduce the industrial/traffic-related

505 emissions in order to alleviate potential health risks.

506 3.6 Limitations and uncertainties

507 It should be noted that our work is still subject to some limitations. At first, some elements

508 such as Cr (0.5) and Ga (0.5) showed relatively lower CV R^2 values though they were generally

509 higher than 0.5. These elements might show the higher uncertainties during the meteorology-

510 normalization compared with other elements such as Cu (0.85) and K (0.85). Besides, few variables

511 were applied to deweather the element concentrations, which might be responsible for the lower CV

512 R^2 value for some elements. Due to the lack of available hourly emission inventory of each element,

513 we only used the time variable to train the model. This method still suffered from some uncertainties,

514 which should be improved by the establishment of near-time emission database.

515 **4. Conclusions and implications**

516 Three-year continuous hourly observation of elements in $PM_{2.5}$ was conducted in Tangshan

517 during September 2017-August 2020. The effect of air clean policy on element concentrations in

518 $PM_{2.5}$ were quantified. The main conclusions were drawn as follows:

(1) The deweathered concentrations of Ga, Co, Pb, Zn, and As showed the rapid decreases from 1.52 to 0.42 ng/m^3 (72%), 1.31 to 0.44 ng/m^3 (67%), 92 to 35 ng/m^3 (62%), 411 to 170 ng/m^3 (59%), and 21 to 10 ng/m^3 (54%), respectively. Clean air actions played the important role on the emission reduction of coal combustion and non-ferrous metal smelting.

(2) The deweathered levels of Ca (8.3%), Cr (19%), and Fe (23%) displayed relatively low decreases compared with other elements, indicating that the vehicle emission and ferrous-smelting industries might be not sensitive to the air clean policy.

(3) The deweathered levels of some elements related with industrial activities (e.g., Ga, Zn, and Cr) exhibited rapid decreases in autumn and winter compared with other seasons during 2017-2020, while the combustion-related elements such as Pb and As did not show high decreasing ratios in winter. The enhanced coal consumption during the heating season offset the benefits derived from strict emission controls measures.

(4) The favorable meteorological conditions promoted the decreases of Ca (-25%), V (-10%), Cr (-2.6%), Mn (-0.68%), Fe (-4.6%), Ni (-7.6%), and Cu (-21%) concentrations.

(5) The contribution ratios of biomass burning, non-ferrous metal smelting, coal combustion, ferrous metal smelting, heavy oil combustion, and traffic-related dust changed from 33%, 11%, 15%, 13%, 3%, and 25% to 33%, 8%, 8%, 13%, 4%, and 33%, respectively.

(6) All of the elements did not show significant noncarcinogenic and carcinogenic risks, while both of As and Pb still displayed relatively high health damages.

Our study presented detailed information about the impact of clean air policy on the chemical compositions and source apportionment of trace elements in PM$_{2.5}$ in Tangshan, and provided new enlightenment for scientific community and policymakers. Many targeted measures could be undertaken to alleviate the air pollution and further to reduce avoided premature health risks. However, this study still suffered some limitations and more steps will be taken toward thoroughly addressing these problems. First of all, the PMF model still showed some uncertainties, and thus characterizing the isotopic signatures of these elements is of great significance. In addition, Sunset OC/EC analyzer, Monitoring of Aerosols and Gases (MARGA) platform, and other on-line measurements should be collocated to probe into the synergistic effect of emission reduction and meteorology on air quality.

550 **Data availability**

551 The boundary layer height dataset was obtained from the website of https://www.ecmwf.int/. The

552 dataset is archived in https://zenodo.org/record/7031975#.Ywys8cjfmfU (Li et al., 2022).

553 **Author contributions**

554 LR wrote the manuscript. LR, PM, ZWD, and HJM contributed to the conceptualization of the study.

555 LR and PM conducted the research, and visualized the results. WGH revised the manuscript.

556 **Competing interests**

557 The contact author has declared that neither they nor their co-authors have any competing interests.

References

D'Alessandro, A., Lucarelli, F., Mandò, P.A., Marcazzan, G., Nava, S., Prati, P., Valli, G., Vecchi, R., Zucchiatti, A.: Hourly elemental composition and sources identification of fine and coarse PM10 particulate matter in four Italian towns. J. Aero. Sci., 34, 243-259, 2003.

Alies, B., Sasaki, I., Proux, O., Sayen, S., Guillon, E., Faller, P., and Hureau, C.: Zn impacts Cu coordination to amyloid-β, the Alzheimer's peptide, but not the ROS production and the associated cell toxicity. Chem. Commun., 49, 1214-1216, 2013.

Alves, C., Gomes, J., Nunes, T., Duarte, M., Calvo, A.I., Custodio, D., Pio, C., Karanasiou, A., and Querol, X.: Size-segregated particulate matter and gaseous emissions from motor vehicles in a road tunnel. Atmos. Res., 153, 134-144, https://doi.org/10.1016/j.atmosres.2014.08.002, 2015.

Ao, M., Qiu, G., Zhang, C., Xu, X., Zhao, L., Feng, X., Qin, S., and Meng, B.: Atmospheric deposition of antimony in a typical mercury-antimony mining area, Shaanxi Province, Southwest China. Environ. Pollut., 245, 173-182, https://doi.org/10.1016/j.envpol.2018.10.125, 2019.

Chang, Y., Huang, K., Xie, M., Deng, C., Zou, Z., Liu, S., and Zhang, Y.: First long-term and near real-time measurement of trace elements in China's urban atmosphere: temporal variability, source apportionment and precipitation effect. Atmos. Chem. Phys., 18, 11793-11812, https://doi.org/10.5194/acp-18-11793-2018, 2018.

Chen, J., Li, C., Ristovski, Z., Milic, A., Gu, Y., Islam, M.S., Wang, S., Hao, J., Zhang, H., and He, C.: A review of biomass burning: Emissions and impacts on air quality, health and climate in China. Sci. Total Environ., 579, 1000-1034, https://doi.org/10.1016/j.scitotenv.2016.11.025, 2017.

Chen, G.B., Li, S.S., Knibbs, L.D., Hamm, N.A.S., Cao, W., Li, T.T., Guo, J.P., Ren, H.Y., Abramson, M.J., and Guo, Y.M.: A machine learning method to estimate $PM_{2.5}$ concentrations across China with remote sensing, meteorological and land use information. Sci. Total Environ., 636, 52-60, https://doi.org/10.1016/j.scitotenv.2018.04.251, 2018.

Clements, A.L., Buzcuguven, B., Fraser, M.P., Kulkarni, P., and Chellam, S.: Role of particulate metals in heterogenous secondary sulfate formation. Atmos. Environ., 75, 233-240, https://doi.org/10.1016/j.atmosenv.2013.04.038, 2013.

Clements, N., Eav, J., Xie, M., Hannigan, M. P., Miller, S. L., Navidi, W., et al.: Concentrations and source insights for traceelements infine and coarse particulate matter. Atmospheric Environment,89, 373–381, https://doi.org/10.1016/j.atmosenv.2014.01.011, 2014.

Cui, L., Duo, B., Zhang, F., Li, C., Fu, H., and Chen, J.: Physiochemical characteristics of aerosol particles collected from the Jokhang Temple indoors and the implication to human exposure. Environ. Pollut., 236, 992-1003, https://doi.org/10.1016/j.envpol.2017.10.107, 2018.

Cui, M., Chen, Y., Feng, Y., Li, C., Zheng, J., Tian, C., Yan, C., and Zheng, M.: Measurement of PM and its chemical composition in real-world emissions from non-road and on-road diesel vehicles. Atmos. Chem. Phys., 17, 6779-6795, https://doi.org/10.5194/acp-17-6779-2017, 2017.

Cui, X., Wang, X., and Liu, B.: The characteristics of heavy metal pollution in surface dust in Tangshan, a heavily industrialized city in North China, and an assessment of associated health risks. J. Geochem. Explor., 210, 106432, 2020.

Cui, Y., Ji, D., Chen, H., Gao, M., Maenhaut, W., He, J., and Wang, Y.: Characteristics and sources of hourly trace elements in airborne fine particles in urban Beijing, China. J. Geophys. Res. Atmos., 124, 11595-11613, https://doi.org/10.1029/2019JD030881, 2019.

Dall'Osto, M., Querol, X., Amato, F., Karanasiou, A., Lucarelli, F., Nava, S., Calzolai, G., and Chiari,

M.: Hourly elemental concentrations in PM$_{2.5}$ aerosols sampled simultaneously at urban background and road site during SAPUSS -diurnal variations and PMF receptor modelling. Atmos. Chem. Phys., 13, 4375-4392, 2013.

Das, R., Mohtar, A.T.B.M., Rakshit, D., Shome, D., and Wang, X.: Sources of atmospheric lead (Pb) in and around an Indian megacity. Atmos. Environ., 193, 57-65, https://doi.org/10.1016/j.atmosenv.2018.08.062, 2018.

Duan, J. and Tan, J.: Atmospheric heavy metals and arsenic in China: situation, sources and control policies. Atmos. Environ., 74, 93-101, 10.1016/j.atmosenv.2013.03.031, 2013.

Fang, B., Zhang, L., Zeng, H., Liu, J., Yang, Z., Wang, H., Wang, Q., and Wang, M.: PM$_{2.5}$-bound polycyclic aromatic hydrocarbons: sources and health risk during non-heating and heating periods (Tangshan, China). Int. J. Env. Res. Pub. He., 17, 483, 2020.

Fernandez, J.A., Rey, A., and Carballeira, A.: An extended study of heavy metal deposition in Galicia (NW Spain) based on moss analysis. Sci. Total Environ., 254, 31-44, 10.1016/s0048-9697(00)00431-9, 2000.

Furger, M., Minguillon, M.C., Yadav, V., Slowik, J.G., Huglin, C., Frohlich, R., Petterson, K., Baltensperger, U., and Prevot, A.S.H.: Elemental composition of ambient aerosols measured with high temporal resolution using an online XRF spectrometer. Atmos. Meas. Technol., 10, 2061-2076, https://doi.org/10.5194/amt-10-2061-2017, 2017.

Geng, G., Xiao, Q., Zheng, Y., Tong, D., Zhang, Y., Zhang, X., Zhang, Q., He, K., and Liu, Y.: Impact of China's air pollution prevention and control action plan on PM$_{2.5}$ chemical composition over eastern China. Sci. China Earth Sci., 62, 1872-1884, https://doi.org/10.1007/s11430-018-9353-x, 2019.

Grivas, G., Cheristanidis, S., Chaloulakou, A., Koutrakis, P., & Mihalopoulos, N.: Elemental composition and source apportionmentoffine and coarse particles at traffic and urban background locations in Athens, Greece.Aerosol and Air Quality Research,18, 1642–1659, 2018.

Guo, J., Tilgner, A., Yeung, C., Wang, Z., Louie, P.K.K., Luk, C.W.Y., Xu, Z., Yuan, C., Gao, Y., and Poon, S.: Atmospheric peroxides in a polluted subtropical environment: seasonal variation, sources and sinks, and importance of heterogeneous processes. Environ. Sci. Technol., 48, 1443-1450, https://doi.org/10.1021/es403229x, 2014.

Harmens, H., Norris, D.A., Steinnes, E., Kubin, E., Piispanen, J., Alber, R., Aleksiayenak, Y., Blum, O., Coskun, M., and Dam, M.: Mosses as biomonitors of atmospheric heavy metal deposition: Spatial patterns and temporal trends in Europe. Environ. Pollut., 158, 3144-3156, https://doi.org/10.1016/j.envpol.2010.06.039, 2010.

He, Q., Zhang, M., Song, Y., and Huang, B.: Spatiotemporal assessment of PM$_{2.5}$ concentrations and exposure in China from 2013 to 2017 using satellite-derived data. J. Cleaner Prod., 286, 124965, https://doi.org/10.1016/j.jclepro.2020.124965, 2021.

Hjortenkrans, D.S., Bergbäck, B.G., and Häggerud, A.V.: Metal emissions from brake linings and tires: case studies of Stockholm, Sweden 1995/1998 and 2005. Environ. Sci. Technol., 41, 5224-5230, https://doi.org/10.1021/es070198o, 2007.

Holden, P.A., Gardeatorresdey, J.L., Klaessig, F., Turco, R.F., Mortimer, M., Hundrinke, K., Hubal, E.A.C., Avery, D., Barcelo, D., and Behra, R.: Considerations of environmentally relevant test conditions for improved evaluation of ecological hazards of engineered nanomaterials. Environ. Sci. Technol., 50, 6124-6145, https://doi.org/10.1021/acs.est.6b00608, 2016.

Huang, C., Bao, L., Luo, P., Wang, Z., Li, S., and Zeng, E.Y.: Potential health risk for residents around a typical e-waste recycling zone via inhalation of size-fractioned particle-bound heavy metals. J

645   Hazard. Mater., 317, 449-456, 10.1016/j.jhazmat.2016.05.081, 2016.

646   Jeong, C., Wang, J.M., and Evans, G.J.: Source apportionment of urban particulate matter using hourly

647   resolved trace metals, organics, and inorganic aerosol components. Atmos. Chem. Phys., 1-32,

648   https://doi.org/10.5194/acp-2016-189, 2016.

649   Kamal, A., Cincinelli, A., Martellini, T., and Malik, R.N.: A review of PAH exposure from the combustion

650   of biomass fuel and their less surveyed effect on the blood parameters. Environ. Sci. Pollut. Res., 22,

651   4076-4098, 10.1007/s11356-014-3748-0, 2015.

652   Kang, S., Chen, P., Li, C., Liu, B., and Cong, Z.: Atmospheric aerosol elements over the inland Tibetan

653   Plateau: concentration, seasonality, and transport. Aerosol Air Qual. Res., 16, 789-800, 2016.

654   Ke, H.B., Gong, S.L., He, J.J., Zhou, C.H., Zhang, L., Zhou, Y.K.: Spatial and temporal distribution of

655   open bio-mass burning in China from 2013 to 2017. Atmospheric Environment., 210, 156-165, 2019.

656   Li, R., Fu, H., Cui, L., Li, J., Wu, Y., Meng, Y., Wang, Y., and Chen, J.: The spatiotemporal variation and

657   key factors of SO_2 in 336 cities across China. J. Cleaner Prod., 210, 602-611,

658   https://doi.org/10.1016/j.jclepro.2018.11.062, 2019.

659   Li, R., Zhao, Y., Fu, H., Chen, J., Peng, M., and Wang, C.: Substantial changes in gaseous pollutants and

660   chemical compositions in fine particles in the North China Plain during the COVID-19 lockdown

661   period: anthropogenic vs. meteorological influences. Atmos. Chem. Phys., 21, 8677-8692,

662   https://doi.org/10.5194/acp-21-8677-2021, 2021.

663   Li, R., Peng, M., Zhao, W.D., Wang, G.H., and Hao, J.M.: Data for "Measurement Report: Rapid changes

664   of chemical characteristics and health risks for high time-resolved trace elements in $PM_{2.5}$ in a typical

665   industrial city in response to stringent clean air actions", [dataset],

666   https://zenodo.org/record/7031975#.Ywys8cjfmfU, 2022.

667   Li, Z., Jiang, J., Ma, Z., Fajardo, O.A., Deng, J., and Duan, L.: Influence of flue gas desulfurization (FGD)

668   installations on emission characteristics of $PM_{2.5}$ from coal-fired power plants equipped with selective

669   catalytic reduction (SCR). Environ. Pollut., 230, 655-662,

670   https://doi.org/10.1016/j.envpol.2017.06.103, 2017.

671   Li, Z., Wang, Y., Li, Z., Guo, S., and Hu, Y.: Levels and sources of $PM_{2.5}$-associated pahs during and after

672   the wheat harvest in a central rural area of the beijing-tianjin-hebei (bth) region. Aerosol Air Qual.

673   Res., 20, 1070-1082, 2020.

674   Lin, Y., Hsu, S., Chou, C.C.K., Zhang, R., Wu, Y., Kao, S., Luo, L., Huang, C., Lin, S., and Huang, Y.:

675   Wintertime haze deterioration in Beijing by industrial pollution deduced from trace metal fingerprints

676   and enhanced health risk by heavy metals. Environ. Pollut., 208, 284-293,

677   https://doi.org/10.1016/j.envpol.2015.07.044, 2016.

678   Liu, H., He, K., Wang, Q., Huo, H., Lents, J., Davis, N., Nikkila, N., Chen, C., Osses, M., and He, C.:

679   Comparison of vehicle activity and emission inventory between Beijing and Shanghai. J. Air Waste

680   Manage., 57, 1172-1177, https://doi.org/10.3155/1047-3289.57.10.1172, 2007.

681   Liu, J., Chen, Y., Chao, S., Cao, H., Zhang, A., and Yang, Y.: Emission control priority of $PM_{2.5}$-bound

682   heavy metals in different seasons: A comprehensive analysis from health risk perspective. Sci. Total

683   Environ., 644, 20-30, https://doi.org/10.1016/j.scitotenv.2018.06.226, 2018a.

684   Liu, R., Men, C., Yu, W., Xu, F., Wang, Q., and Shen, Z.: Uncertainty in positive matrix factorization

685   solutions for PAHs in surface sediments of the Yangtze River Estuary in different seasons.

686   Chemosphere 191, 922-936, https://doi.org/10.1016/j.chemosphere.2017.10.070, 2018b.

687   Lopez-Cruz, J., Crespo-Salvador, O., Fernandez-Crespo, E., Garcia-Agustin, P., and Gonzalez-Bosch, C.:

688   Absence of Cu-Zn-superoxide dismutase BCSOD1 reduces Botrytis cinerea virulence in Arabidopsis

and in tomato plants, which reveals interplay among ROS, callose and signaling pathways. Mol. Plant Pathol., 18, 16-31, 2016.

Lyu, X.P., Chen, N., Guo, H., Zeng, L.W., Zhang, W.H., Shen, F., Quan, J.H., Wang, N.: Chemical characteristics and causes of airborne particulate pollution in warm seasons in Wuhan, central China. Atmos. Chem. Phys. 16, 10671–10687, www.atmos-chem-phys.net/16/10671/2016/, 2016

Lyu, Y., Zhang, K., Chai, F., Cheng, T., Yang, Q., Zheng, Z., and Li, X.: Atmospheric size-resolved trace elements in a city affected by non-ferrous metal smelting: Indications of respiratory deposition and health risk. Environ. Pollut., 224, 559-571, https://doi.org/10.1016/j.envpol.2017.02.039, 2017.

Ma, Z., Liu, R., Liu, Y., and Bi, J.: Effects of air pollution control policies on $PM_{2.5}$ pollution improvement in China from 2005 to 2017: a satellite-based perspective. Atmos. Chem. Phys., 19, 6861-6877, https://doi.org/10.5194/acp-19-6861-2019, 2019.

Manju, A., Kalaiselvi, K., Dhananjayan, V., Palanivel, M., Banupriya, G., Vidhya, M., Panjakumar, K., and Ravichandran, B.: Spatio-seasonal variation in ambient air pollutants and influence of meteorological factors in Coimbatore, southern India. Air Qual. Atmos. Heal., 11, 1179-1189, https://doi.org/10.1007/s11869-018-0617-x, 2018.

Manousakas, M., Papaefthymiou, H., Diapouli, E., Migliori, A., Karydas, A.G., Bogdanovic-radovic Radovic, I., and Eleftheriadis, K.: Assessment of $PM_{2.5}$ sources and their corresponding level of uncertainty in a coastal urban area using EPA PMF 5.0 enhanced diagnostics. Sci. Total Environ. 574, 155-164, 2017.

Micheline, G., Rachida, C., Celine, M., Gaby, K., Rachid, A., and Petru, J.: Levels of Pb, Cd, Hg and As in fishery products from the eastern Mediterranean and human health risk assessment due to their Consumption. Interna. J. Environ. Res., 13, 443-455, https://doi.org/10.1007/s41742-019-00185-w, 2019.

Moreno, T., Querol, X., Alastuey, A., La Rosa, J.D.D., La Campa, A.M.S.D., Minguillon, M., Pandolfi, M., Gonzalez-castanedo Castanedo, Y., Monfort, E., and Gibbons, W.: Variations in vanadium, nickel and lanthanoid element concentrations in urban air. Sci. Total Environ., 408, 4569-4579, https://doi.org/10.1016/j.scitotenv.2010.06.016, 2010.

Oldani, K.M., Mladenov, N., Williams, M., Campbell, C.M., and Lipson, D.A.: Seasonal patterns of dry deposition at a high-elevation site in the colorado rocky mountains. J. Geophys. Res. Atmos., 122, 2017.

Olujimi, O.O., Oputu, O., Fatoki, O.S., Opatoyinbo, O.E., Aroyewun, O.A., and Baruani, J.: Heavy metals speciation and human health risk assessment at an illegal gold mining site in Igun, Osun State, Nigeria. J. Health. Pollut., 5, 19-32, 2015.

Paatero, P. and Tapper, U.: Positive matrix factorization: A non-negative factor model with optimal utilization of error estimates of data values. Environmetrics 5, 111-126, 1994.

Pacyna, J.M. and Pacyna, E.G.: An assessment of global and regional emissions of trace metals to the atmosphere from anthropogenic sources worldwide. Environ. Rev., 9, 269-298, 2001.

Prati, P., Zucchiatti, A., Lucarelli, F., Mandò, P.A.: Source apportionment near a steel plant in Genoa (Italy) by continuous aerosol sampling and PIXE analysis. Atmos. Environ., 34, 3149-3157, 2000.

Rai, P.K., Lee, S.S., Zhang, M., Tsang, Y.F., and Kim, K.: Heavy metals in food crops: Health risks, fate, mechanisms, and management. Environ. Interna., 125, 365-385, 2019.

Rasmussen, P.E.: Long-range atmospheric transport of trace metals: the need for geoscience perspectives. Environ. Earth Sci., 33, 96-108, 1998.

Reff, A., Eberly, S.I., and Bhave, P.V.: Receptor modeling of ambient particulate matter data using

733   positive matrix factorization: review of existing methods. J. Air Waste Manage., 57, 146-154, 2007.

734 Ren, Z., Zhang, B., Lu, P., Li, C., Gao, L., and Zheng, M.: Characteristics of air pollution by
735   polychlorinated dibenzo-p-dioxins and dibenzofurans in the typical industrial areas of Tangshan City,
736   China. J. Environ. Sci. -China, 23, 228-235, 2011.

737 Saffari, A., Daher, N., Shafer, M.M., Schauer, J.J., and Sioutas, C.: ~~global~~ Global perspective on the
738   oxidative potential of airborne particulate matter: a synthesis of research findings. Environ. Sci.
739   Technol., 48, 7576-7583, 2014.

740 Shafer, M.M., Toner, B.M., Overdier, J.T., Schauer, J.J., Fakra, S.C., Hu, S., Herner, J.D., and Ayala, A.:
741   Chemical speciation of vanadium in particulate matter emitted from diesel vehicles and urban
742   atmospheric aerosols. Environ. Sci. Technol., 46, 189-195, 2012.

743 Shi, G., Teng, J., Ma, H., Li, Y., and Sun, B.: Metals and metalloids in precipitation collected during
744   CHINARE campaign from Shanghai, China, to Zhongshan Station, Antarctica: Spatial variability and
745   source identification. Global Biogeochem. Cyc., 29, 760-774, 2015.

746 Storelli, M.M.: Potential human health risks from metals (Hg, Cd, and Pb) and polychlorinated biphenyls
747   (PCBs) via seafood consumption : estimation of target hazard quotients (THQs) and toxic equivalents
748   (TEQs). Food and Chemical Toxicology 46, 2782-2788, 2008.

749 Taghvaee, S., Sowlat, M.H., Mousavi, A., Hassanvand, M.S., Yunesian, M., Naddafi, K., and Sioutas, C.:
750   Source apportionment of ambient $PM_{2.5}$ in two locations in central Tehran using the Positive Matrix
751   Factorization (PMF) model. Sci. Total Environ., 628-629, 672-686, 2018.

752 Tang, Q., Sheng, W., Li, L., Zheng, L., Miao, C., and Sun, R.: Alteration behavior of mineral structure
753   and hazardous elements during combustion of coal from a power plant at Huainan, Anhui, China.
754   Environ. Pollut., 239, 768-776, 2018.

755 Tian, H., Zhu, C., Gao, J., Cheng, K., Hao, J., Wang, K., Hua, S., Wang, Y., and Zhou, J.: Quantitative
756   assessment of atmospheric emissions of toxic heavy metals from anthropogenic sources in China:
757   historical trend, spatial distribution, uncertainties, and control policies. Atmos. Chem. Phys., 15,
758   10127-10147, 2015.

759 Tianxue, W., Yuesi, W., Shihyu, C., and Guangren, L.: On-line measurement of water-soluble ions in
760   ambient particles. Adv. Atmos. Sci., 23, 586-592, 2006.

761 Wang, S., Su, H., Chen, C., Tao, W., Streets, D.G., Lu, Z., Zheng, B., Carmichael, G.R., Lelieveld, J.,
762   and Pöschl, U.: Natural gas shortages during the "coal-to-gas" transition in China have caused a large
763   redistribution of air pollution in winter 2017. P. Natl. Acad. Sci. USA, 117, 31018-31025, 2020a.

764 Wang, S., Su, H., Chen, C., Tao, W., Streets, D.G., Lu, Z., Zheng, B., Carmichael, G.R., Lelieveld, J.,
765   Pöschl, U., and Cheng, Y.: Natural gas shortages during the "coal-to-gas" transition in China have
766   caused a large redistribution of air pollution in winter 2017. P. Natl. Acad. Sci. USA, 117, 31018-
767   31025, 2020b.

768 Westerdahl, D., Wang, X., Pan, X., and Zhang, K.M.: Characterization of on-road vehicle emission
769   factors and microenvironmental air quality in Beijing, China. Atmos. Environ., 43, 697-705,
770   https://doi.org/10.1016/j.atmosenv.2008.09.042, 2009.

771 Witt, M.L.I., Baker, A.R., and Jickells, T.D.: Atmospheric trace metals over the Atlantic and South Indian
772   Oceans: Investigation of metal concentrations and lead isotope ratios in coastal and remote marine
773   aerosols. Atmos. Environ., 40, 5435-5451, https://doi.org/10.1016/j.atmosenv.2006.04.041, 2006.

774 Wu, Q., Wang, S., Zhang, L., Song, J., Yang, H., and Meng, Y.: Update of mercury emissions from China's
775   primary zinc, lead and copper smelters, 2000-2010. Atmos. Chem. Phys., 12, 18207-18242,
776   https://doi.org/10.5194/acp-12-11153-2012, 2012.

777   Wu, Y., Wang, R., Zhou, Y., Lin, B., Fu, L., He, K., and Hao, J.: ~~on~~On-road vehicle emission control in
778   beijing: past, present, and future. Environ. Sci. Technol., 45, 147-153,
779   https://doi.org/10.1021/es1014289, 2011.

780   Xiao, Q., Geng, G., Liang, F., Wang, X., Lv, Z., Lei, Y., Huang, X., Zhang, Q., Liu, Y., and He, K.:
781   Changes in spatial patterns of $PM_{2.5}$ pollution in China 2000-2018: Impact of clean air policies.
782   Environ. Interna., 141, 105776, https://doi.org/10.1016/j.envint.2020.105776, 2020.

783   Yang, Q., Yuan, Q., Li, T., Shen, H., and Zhang, L.: The relationships between $PM_{2.5}$ and meteorological
784   factors in China: seasonal and regional variations. Int. J. Env. Res. Pub. He., 14, 1510, 2017.

785   Yi, Y., Yang, Z., and Zhang, S.: Ecological risk assessment of heavy metals in sediment and human health
786   risk assessment of heavy metals in fishes in the middle and lower reaches of the Yangtze River basin.
787   Environ. Pollut., 159, 2575-2585, https://doi.org/10.1016/j.envpol.2011.06.011, 2011.

788   Yu, L., Wang, G., Zhang, R., Zhang, L., Song, Y., Wu, B., Li, X., An, K., and Chu, J.: ~~characterization~~
789   Characterization and source apportionment of $pm_{2.5}$ in an urban environment in beijing. Aerosol Air
790   Qual. Res., 13, 574-583, doi: 10.4209/aaqr.2012.07.0192, 2013.

791   Song, Z.F.: An assessment of the heavy metal pollution and potential ecological hazards in urban soil of
792   Tangshan City. Geology in China 38, 1379-1386, 2011.

793   Zhang, J., Zhou, X., Wang, Z., Yang, L., Wang, J., Wang, W.: Trace elements in $PM_{2.5}$ in Shandong
794   Province: Source identification and health risk assessment. Science of the Total Environment 621,
795   558-577, 2018.

796   Zhang, Q., Zheng, Y., Tong, D., Shao, M., Wang, S., Zhang, Y., Xu, X., Wang, J., He, H., Liu, W., Ding,
797   Y., Lei, Y., Li, J., Wang, Z., Zhang, X., Wang, Y., Cheng, J., Liu, Y., Shi, Q., Yan, L., Geng, G., Hong,
798   C., Li, M., Liu, F., Zheng, B., Cao, J., Ding, A., Gao, J., Fu, Q., Huo, J., Liu, B., Liu, Z., Yang, F., He,
799   K., and Hao, J.: Drivers of improved $PM_{2.5}$ air quality in China from 2013 to 2017. P. Natl. Acad. Sci.
800   USA, 116, 24463-24469, https://doi.org/10.1073/pnas.1907956116, 2019.

801   Zhao, M., Zhang, Y., Ma, W., Fu, Q., Yang, X., Li, C., Zhou, B., Yu, Q., and Chen, L.: Characteristics
802   and ship traffic source identification of air pollutants in China's largest port. Atmos. Environ., 64, 277-
803   286, https://doi.org/10.1016/j.atmosenv.2012.10.007, 2013.

804   Zhu, C., Tian, H., Hao, Y., Gao, J., Hao, J., Wang, Y., Hua, S., Wang, K., and Liu, H.: A high-resolution
805   emission inventory of anthropogenic trace elements in Beijing-Tianjin-Hebei (BTH) region of China.
806   Atmos. Environ., 191, 452-462, https://doi.org/10.1016/j.atmosenv.2018.08.035, 2018.

807   Zhu, C., Tian, H., and Hao, J.: Global anthropogenic atmospheric emission inventory of twelve typical
808   hazardous trace elements, 1995–2012. Atmos. Environ., 220, 117061,
809   https://doi.org/10.1016/j.atmosenv.2019.117061, 2020.

810

设置了格式: 下标

Figure 1 The topographic map of China indicating the location of Tangshan (a), sampling site (b), and some major industrial points (b). The population distribution of Tangshan is also depicted in (b).
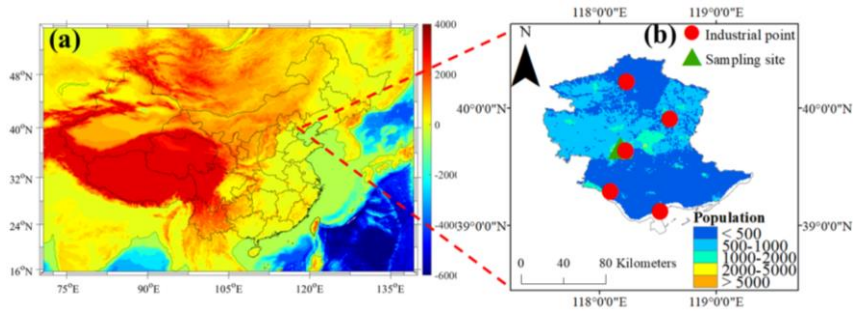
Figure 2 The bar chart of the concentrations of 16 trace elements including K, Fe, Ca, Zn, Pb, Mn,

Fe, As, Se, V, Cr, Ag, Ni, Hg, Ga, and Co.

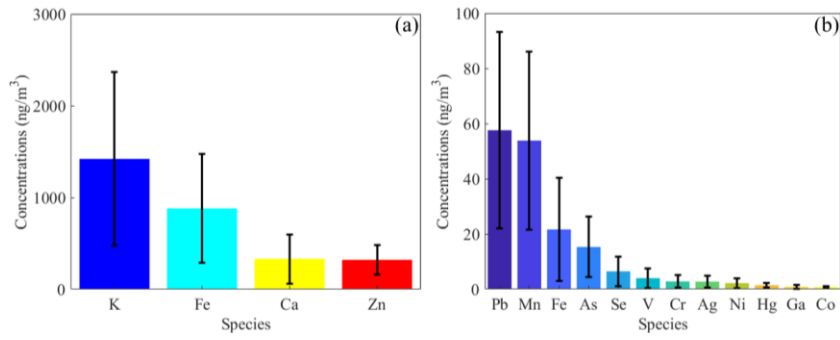**Figure 3** Inter-annual variations of original (red) and deweathered (manganese purple) element concentrations (ng/m^3) in PM$_{2.5}$ in Tangshan. The dark, nattier blue, and nattier yellow backgrounds represent the species during 2017-2018 (from September in 2017 to August in 2018), 2018-2019 (from September in 2018 to August in 2019), and 2019-2020 (from September in 2019 to August in 2020).
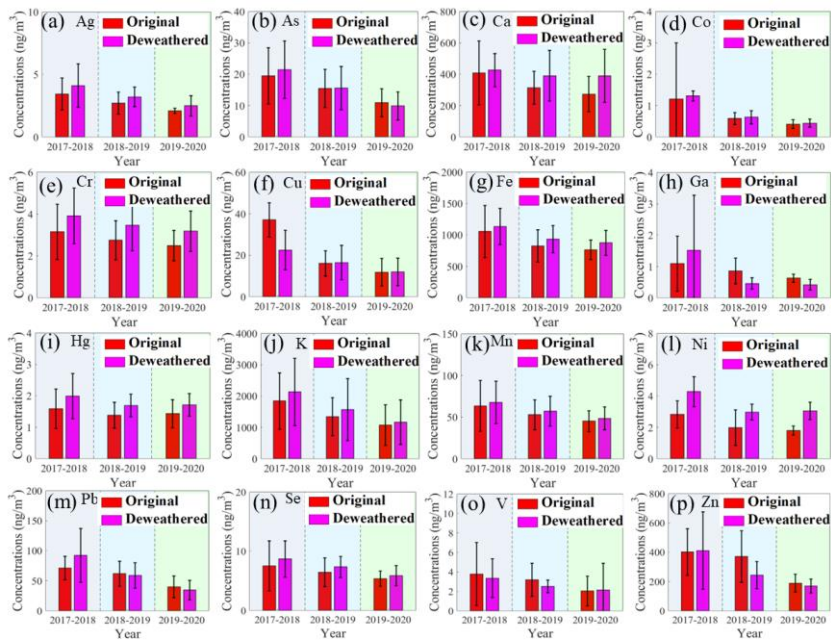
Figure 4 The original (red and orange) and deweathered (green and blue) element concentrations (ng/m^3) in PM$_{2.5}$ in Tangshan in four seasons during 2017-2018, 2018-2019, and 2019-2020. S1, U1, A1, and W1 represent the spring, summer, autumn, and winter during 2017-2018. S2, U2, A2, and W2 denote the spring, summer, autumn, and winter during 2018-2019. S3, U3, A3, and W3 are the spring, summer, autumn, and winter during 2019-2020.
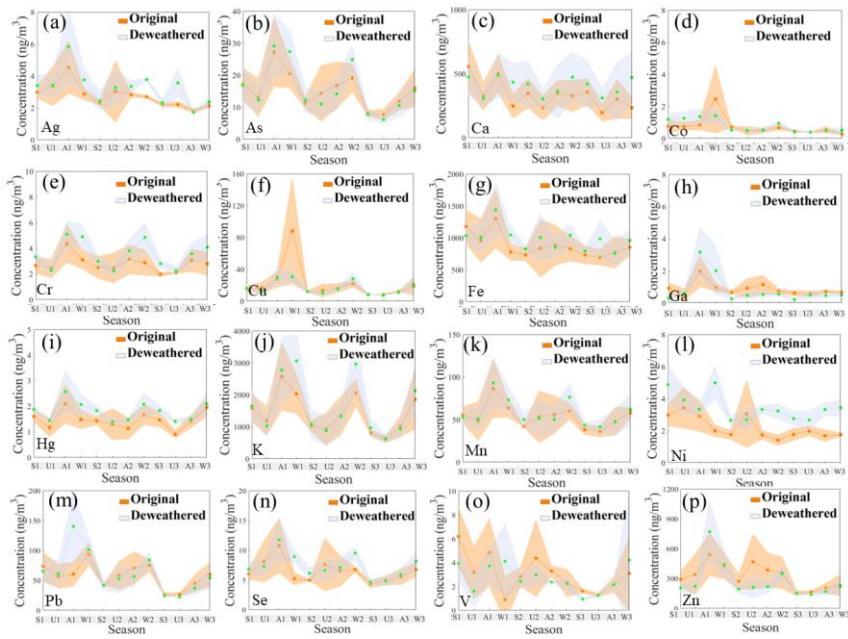
Figure 5 Weekly variations of original (green) and deweathered (orange) element concentrations (ng/m^3) in PM$_{2.5}$ in Tangshan. The green and dark backgrounds denote the error bars of original and deweathered elements, respectively.
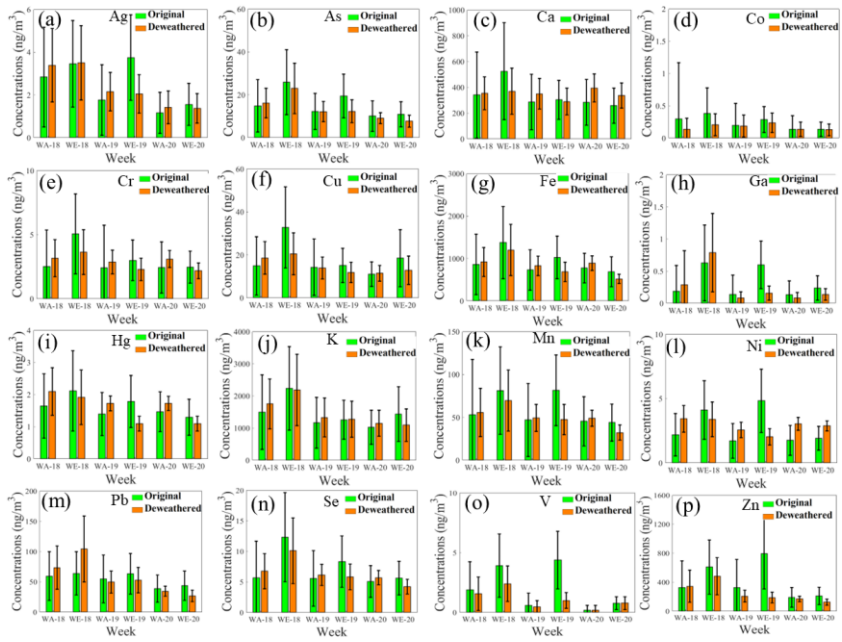
Figure 6 Relative importance of the predictors for the prediction of trace elements. The columns in the figure represent the variable importance in RF models for trace elements. P, RH, T, WD, WS, DOW, HOY, DOY, and Year denote air pressure, relative humidity, air temperature, wind direction, wind speed, day of week, hour of day, day of year, and study year, respectively.
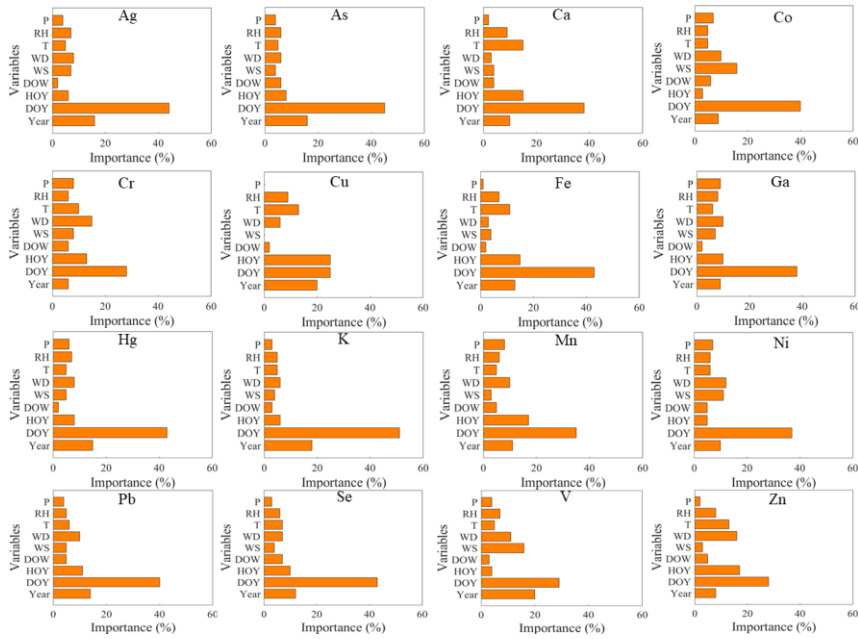
Figure 7 The deweathered concentrations of trace elements derived from six sources in Tangshan during 2017-2020.
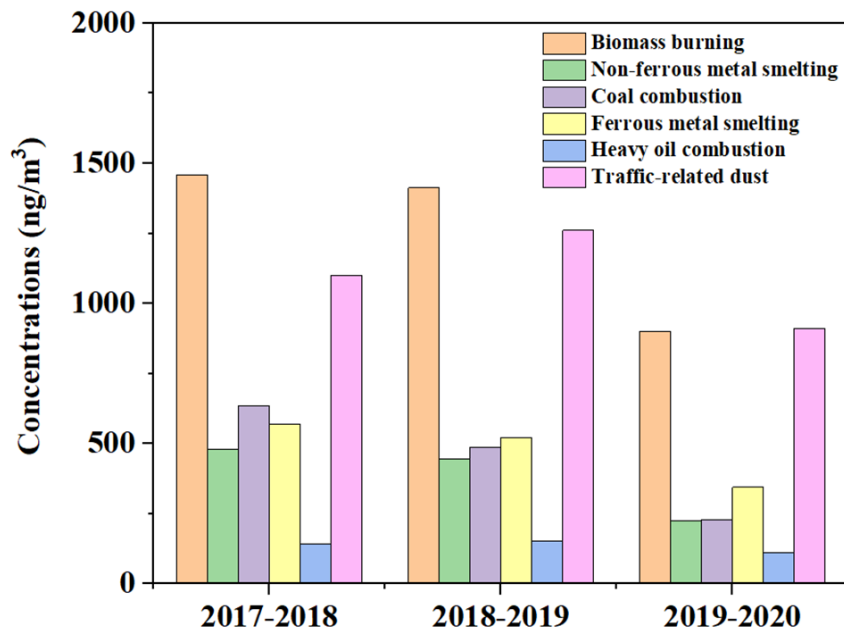
Figure 8 Average contributions of six sources to the deweathered concentrations of elements in PM$_{2.5}$ based on PMF model. The red panel means the biomass burning; the green panel denotes the non-ferrous metal smelting; the blue one represents the coal combustion; the cyan one is the ferrous metal smelting; the pink one represents the heavy oil combustion; and the yellow one denotes the traffic-related dust. (a), (b), and (c) represent the source contributions during 2017-2018, 2018-2019, and 2019-2020, respectively.
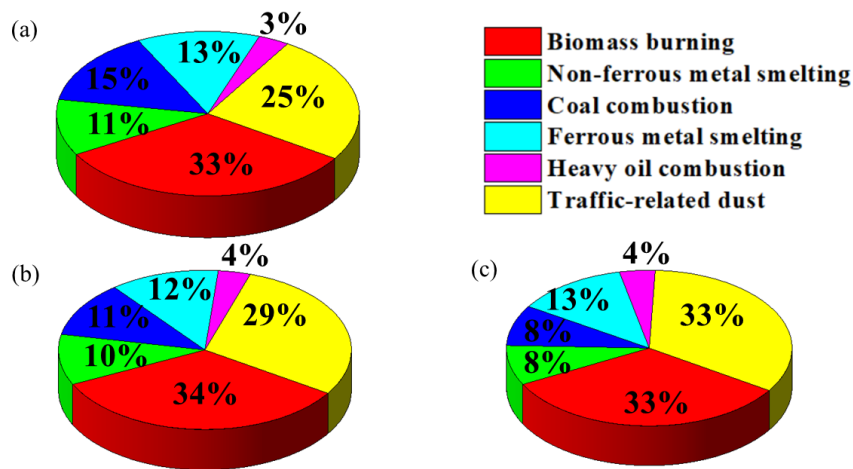
Table 1 The comparison of element concentrations in PM$_{2.5}$ of Tangshan and the standard values for these elements in World Health Organization (WHO), China, Europe, and the United States.

Elements	Mean±SD	CAAQS	WHO	EU	United States
Co	0.74±0.24				
Ga	0.86±0.74				
Hg	1.47±0.81	50	1000		
Ni	2.21±1.80		25	20	
Ag	2.75±2.08				
Cr	2.80±2.22	0.025	0.25		
V	3.98±3.57				
Se	6.46±5.28				
As	15.3±11.0	6	6.60	6	
Cu	21.7±18.7				
Mn	53.8±32.3				
Pb	57.6±35.7		1000		150
Zn	320±162				
Ca	332±268				
Fe	881 ± 591				
K	1421±947				

Table 2 The non-carcinogenic and carcinogenic risks for the original element levels in PM$_{2.5}$.

Age	Year	Indicator	Cr	Mn	Fe	Co	Ni	Cu	Zn	As	Pb
Adult	2017-2018	HQ	2.47×10^{-4}	1.07×10^{-4}	3.55×10^{-4}	4.50×10^{-4}	0.33×10^{-4}	1.18×10^{-4}	3.15×10^{-4}	1.53×10^{-2}	8.39×10^{-4}
		CR	0.13×10^{-6}	--	--	--	--	--	--	2.37×10^{-6}	2.88×10^{-6}
	2018-2019	HQ	2.16×10^{-4}	0.89×10^{-4}	2.77×10^{-4}	4.67×10^{-4}	0.23×10^{-4}	0.95×10^{-4}	2.91×10^{-4}	1.21×10^{-2}	7.28×10^{-4}
		CR	0.11×10^{-6}	--	--	--	--	--	--	1.87×10^{-6}	2.50×10^{-6}
	2019-2020	HQ	1.95×10^{-4}	0.76×10^{-4}	2.58×10^{-4}	3.26×10^{-4}	0.21×10^{-4}	0.70×10^{-4}	1.49×10^{-4}	0.86×10^{-2}	4.69×10^{-4}
		CR	0.10×10^{-6}	--	--	--	--	--	--	1.33×10^{-6}	1.61×10^{-6}
Child	2017-2018	HQ	6.02×10^{-4}	2.60×10^{-4}	8.64×10^{-4}	11.1×10^{-4}	0.81×10^{-4}	2.87×10^{-4}	7.67×10^{-4}	3.73×10^{-2}	20.4×10^{-4}
		CR	0.08×10^{-6}	--	--	--	--	--	--	1.44×10^{-6}	1.75×10^{-6}
	2018-2019	HQ	5.26×10^{-4}	2.17×10^{-4}	6.74×10^{-4}	11.0×10^{-4}	0.57×10^{-4}	2.30×10^{-4}	7.08×10^{-4}	2.95×10^{-2}	17.7×10^{-4}
		CR	0.07×10^{-6}	--	--	--	--	--	--	1.14×10^{-6}	1.52×10^{-6}

| 2019-2020 | HQ | $4.75×10^{-4}$ | $1.85×10^{-4}$ | $6.27×10^{-4}$ | $7.93×10^{-4}$ | $0.52×10^{-4}$ | $1.70×10^{-4}$ | $3.61×10^{-4}$ | $2.09×10^{-2}$ | $11.4×10^{-4}$ |
| | CR | $0.06×10^{-6}$ | -- | -- | -- | -- | -- | -- | $0.81×10^{-6}$ | $0.98×10^{-6}$ |

Table 3 The non-carcinogenic and carcinogenic risks for the deweathered element levels in PM$_{2.5}$.

Age	Year	Indicator	Cr	Mn	Fe	Co	Ni	Cu	Zn	As	Pb
Adult	2017-2018	HQ	3.07×10^{-4}	1.14×10^{-4}	3.82×10^{-4}	10.3×10^{-4}	0.50×10^{-4}	1.33×10^{-4}	3.15×10^{-4}	1.68×10^{-2}	10.8×10^{-4}
		CR	0.16×10^{-6}	--	--	--	--	--	--	2.60×10^{-6}	3.72×10^{-6}
	2018-2019	HQ	2.73×10^{-4}	0.96×10^{-4}	3.14×10^{-4}	4.93×10^{-4}	0.35×10^{-4}	0.97×10^{-4}	2.91×10^{-4}	1.22×10^{-2}	6.91×10^{-4}
		CR	0.14×10^{-6}	--	--	--	--	--	--	1.89×10^{-6}	2.37×10^{-6}
	2019-2020	HQ	2.50×10^{-4}	0.82×10^{-4}	2.95×10^{-4}	3.46×10^{-4}	0.36×10^{-4}	0.70×10^{-4}	1.49×10^{-4}	0.78×10^{-2}	4.08×10^{-4}
		CR	0.13×10^{-6}	--	--	--	--	--	--	1.20×10^{-6}	1.40×10^{-6}
Child	2017-2018	HQ	7.47×10^{-4}	2.77×10^{-4}	9.28×10^{-4}	11.7×10^{-4}	1.23×10^{-4}	3.22×10^{-4}	3.23×10^{-4}	4.09×10^{-2}	26.4×10^{-4}
		CR	0.10×10^{-6}	--	--	--	--	--	--	1.58×10^{-6}	2.26×10^{-6}
	2018-2019	HQ	6.64×10^{-4}	2.34×10^{-4}	7.64×10^{-4}	11.9×10^{-4}	0.85×10^{-4}	2.36×10^{-4}	1.91×10^{-4}	2.98×10^{-2}	16.8×10^{-4}
		CR	0.09×10^{-6}	--	--	--	--	--	--	1.15×10^{-6}	1.44×10^{-6}

2019-2020	HQ	6.08×10^{-4}	1.99×10^{-4}	7.17×10^{-4}	8.42×10^{-4}	0.87×10^{-4}	1.71×10^{-4}	1.34×10^{-4}	1.89×10^{-2}	9.92×10^{-4}
	CR	0.08×10^{-6}	--	--	--	--	--	--	0.73×10^{-6}	0.85×10^{-6}